Nano-twines to perpendicular lateral protrusions: Role of force exerting perpendicular lateral protrusions in fibroblastic cell contraction

Authors:

Abinash Padhi[1], Karanpreet Singh[2], Janusz Franco-Barraza[3], Daniel J. Marston[4], Klaus M. Hahn[4], Edna Cukierman[3], Rakesh K. Kapania[2], and Amrinder S. Nain[1 *]

[1] Department of Mechanical Engineering, Virginia Tech, Blacksburg, Virginia, USA

[2] Department of Aerospace and Ocean Engineering, Virginia Tech, Blacksburg, Virginia, USA

[3] Cancer Biology Program, Marvin & Concetta Greenberg Pancreatic Cancer Institute, Fox Chase Cancer Center, USA

[4] Department of Pharmacology, The University of North Carolina at Chapel Hill, Chapel Hill, NC 27599

* Corresponding Author: nain@vt.edu

Keywords: Lateral protrusions, protrusive forces, aligned fibers, cell forces, cell protrusions, desmoplasia

ABSTRACT

Aligned extracellular matrix fibers impart an elongated cell morphology and enable fibroblasts to undergo myofibroblastic activation. Yet the biomechanical intricacies that are associated with this microenvironmental phenomenon are unknown. Here, we identify a new role of lateral protrusions, originating anywhere along elongated fibroblastic cells, which apply fiber-deflecting contractile forces. Using aligned fiber networks that serve as force sensors, we quantitate the role of lateral nano-projections (twines) that mature into “perpendicular lateral protrusions” (PLPs) through the formation of twine-bridges, thus allowing elongated cells to spread laterally and effectively contract. Using quantitative microscopy at high spatiotemporal resolution, we show that twines of varying lengths can originate from stratification of cyclic actin waves traversing along the entire length of the cell. Primary twines swing freely in 3D and engage with neighboring extracellular fibers in interaction times of seconds. Once engaged, an actin lamellum grows along the length of primary twine and re-stratifies to form a secondary twine. Engagement of secondary twine with the neighboring fiber leads to the formation of twine-bridge, a critical step in providing a conduit for actin to advance along and populate the twine-bridge. Through arrangement of fiber networks in varying configurations, we confirm that anisotropic fibrous environments are fertile for PLP dynamics, and importantly force-generating PLPs are oriented perpendicular to the parent cell body. Furthermore, cell spreading onto multiple fibers and myofibroblastic-like contraction occur through PLPs. Our identification of force exertion by PLPs identifies a possible explanation for cancer-associated desmoplastic expansion, at single-cell resolution, thus providing new clinical intervention opportunities.

INTRODUCTION

During acute wound healing, myofibroblastic activation of local and/or recruited fibroblastic cells imparts inward forces and contracts the collagen-rich extracellular matrix (ECM) that, upon wound resolution, comprises the acellular scar. Importantly, myofibroblastic cell contraction is not just pivotal to many physiological (e.g., developmental, acute wound healing) processes, but it is also key to numerous pathological occurrences (e.g., chronic inflammation and fibrosis-related diseases including microenvironmental desmoplasia in solid cancers)[1,2]. It is thus not surprising that cancers have been described as chronic wounds for which desmoplasia, the contractile fibrous-like tumor-microenvironment, plays a pivotal role during both tumor onset and progression[3,4]. In solid epithelial tumors, desmoplasia expands in a manner it simulates chronic wound extension[5]. In fact, in extreme cases, such as in pancreatic ductal adenocarcinomas (PDAC), desmoplasia can expand in a way that it encompasses the majority of the tumor mass[6]. Interestingly, just as scarred tissue often presents with aligned collagen signatures, aligned ECM fibers described as "tumor-associated collagen" or TAC signatures, were described as hallmarks of desmoplasia by the late Patricia Keely, who demonstrated that aligned TACs associated with detrimental patient outcomes[7–10]. Importantly, myofibroblastic cancer associated fibroblasts, or myCAFs, are known to be the local force-dependent activated cells responsible for the production and remodeling of the topographically aligned, anisotropic, desmoplastic ECM. Of note, we have previously demonstrated that anisotropic ECMs generated by CAFs, can activate naïve fibroblastic cells into myCAFs[11], suggesting that CAF generated aligned ECMs could drive desmoplastic expansion. Despite vast data available regarding the role of aligned ECMs in enabling polarized migration[8,12–16], very little is known about ECM-dependent desmoplastic expansion. To this end, it is commonly understood that in aligned ECMs, cell elongation and polarity (i.e., throughout cell migration) is maintained due to minimal probing in lateral directions[15]. In such scenarios, how cells stretch onto multiple-fibers and whether spreading is driven primarily by leading edge probing, or through the formation of force exerting lateral protrusions along the cell body that could then contract inwards to aid in desmoplastic remodeling remain poorly understood. This study attempts to fill gaps regarding the manner that aligned ECM triggers desmoplastic expansion via a new type of contractile lateral fibroblastic cell protrusions.

Lateral protrusions or spikes are well-documented in multiple cell types (growth cones, mesenchymal, fibrosarcoma, hepatocytes, and conjunctival cells)[17,18] in varying sizes (2-10 μm in length and 0.2-0.5 μm diameter).[18,19] These structures have been implicated in the proteolytic degradation of the 3D interstitial ECM by cancer cells[18], and by leukocytes in probing the vascular membrane for permissive sites which eventually allows emigration into extravascular tissue[20]. In the case of leukocytes in the presence of shear flow, cells exhibit rolling via tethering by the formation of transient receptor-ligand bonds.[21,22] These are facilitated by microvilli shown to be 80nm in diameter and varying in length from 350 nm to 1 μm or longer[23,24]. Similarly, lateral protrusions formed in melanoma cells have also been documented to provide traction in a 3D environment in the absence of adhesion.[25] It was recently shown that spindle-shaped cells in 3D gel matrices form fewer lateral protrusions,[26] which is attributed to restriction in α5β1 integrin recycling to protrusions at leading edge [15,27], and or RhoA activation away from the leading edge which inhibits Rac1 thereby preventing the formation of lateral protrusions, thus helping maintain cell polarity and directed migration.[27–29] Overall, the utility of lateral protrusions remains partially understood as current cell culturing methods of classic 2D culturing limit the formation of lateral protrusions, while 3D gels lack the homogeneity and topographic patterning that are needed to study them in a reproducible manner. To this end, using fiber diameters of curvature contrast, we have recently shown the ability to study lateral protrusions of various shapes and sizes, formed in an integrin-dependent manner, on fibers of different diameters[30]. Here, using aligned and suspended fiber nanonets that also act as force sensors, we report that elongated cells (of different lineages) can form lateral protrusions that swing freely in 3D and that these attach to neighboring ECM fibers in a matter of seconds. These filamentous lateral protrusions (primary *twines*), originating from the stratification of actin waves, act as catalysts for the formation of *secondary twines*. We

show that suspended *twine-bridges,* composed of primary-secondary twines oriented perpendicular to cell body, mature into lamellipodial resembling structures we named “perpendicular lateral protrusions” (PLPs, **Figure 1**), which are capable of exerting forces that enable cells to spread in the transverse direction. Cell spreading on multiple fibers increases their contractility, which decreases the migration speed. Altogether, we quantitatively describe anisotropic ECMs to promote production of PLPs that enables fibroblastic cell contraction thus explaining, for the first time, physical characteristics of desmoplastic expansion.

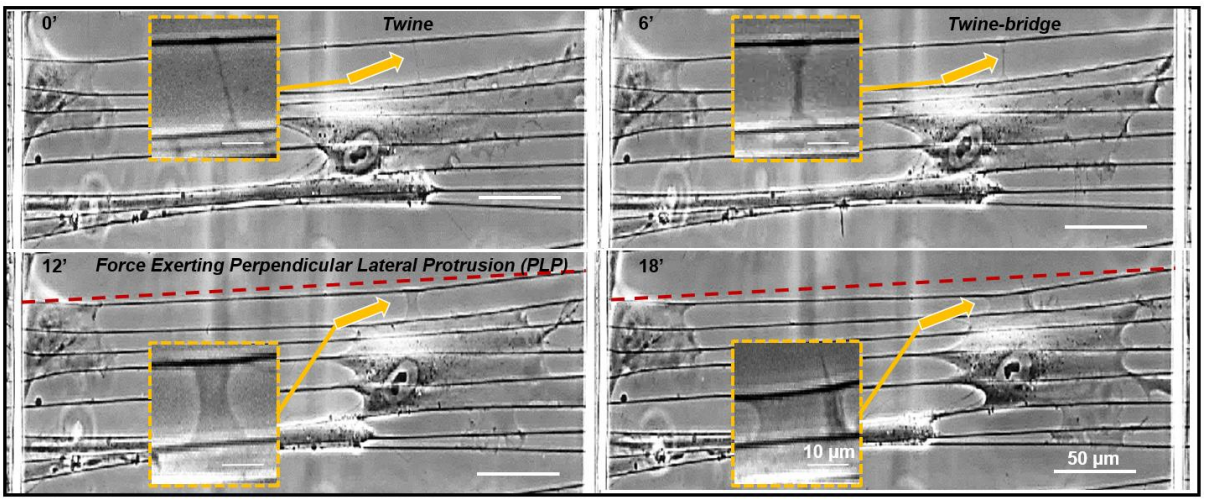

FIGURE 1. Nano-twines to perpendicular lateral protrusions (PLPs). Timelapse images of single cell in elongated shape spreading laterally through force exerting PLPs on neighboring fibers (Movie M1). Twines mature to form *twine-bridges* that are capable of applying inward contractile forces. Insets shows magnified images and dashed red line shows undeflected position of fiber.

RESULTS and DISCUSSIONS

Twines emerge from actin ruffles and engage neighboring fiber in seconds

We inquired if lateral protrusions could form in elongated cells, and used the previously described non-electrospinning (Spinneret based Tunable Engineered Parameters, STEP[31–33]) method to fabricate anisotropically/aligned fibers that also served as force sensing nanonets[34,35]. We hence followed, in real-time, the spreading and cellular protrusive occurrences of fibroblastic immortalized murine (C2C12, embryonic fibroblast (MEF), and well established NIH 3T3) and human mesenchymal stem cells (hMSCs) as well as Hela cells, using transmitted phase-contrast microscopy (**Supplementary figure S1**). All cell types acquired an elongated shape, as expected, while continuously forming nano-filamentous structures, termed *twines* (shown by yellow arrows in **Figure 1**), located lateral to the polarized direction (i.e., long axis) of the cell. The *twines* were seen to attach to neighboring fibers, become thicker (mature) and apply contractile forces evidenced by deflection of neighboring fiber (**Movie M1**). We found that *twines* originated from membrane ruffles that resembled previously described cyclic actin waves[36]. The membrane ruffles spiraled about the fiber axis (**Figure 2A** and **Movie M2**) and advanced at 6.58 µm/min (n=30) similar to actin polymerization rates reported in the literature (7.20-8.73 µm/min).[37] The ruffles extended beyond the main cell body and stratified into denser independent twines (**Figure 2B** and **Movie M3**) presumably due to folding-over and buckling.[38] The *twines* were found to grow in length at the rate of ~0.1 µm/s, and swing freely (in 3D) similarly to reported angular rotations of filopodia,[39–42] which allowed for selected ones to engage (attach) to a neighboring fiber. The attachment to neighboring fiber occurred in a matter of seconds (**Figure 2C** and **Movie M4**).

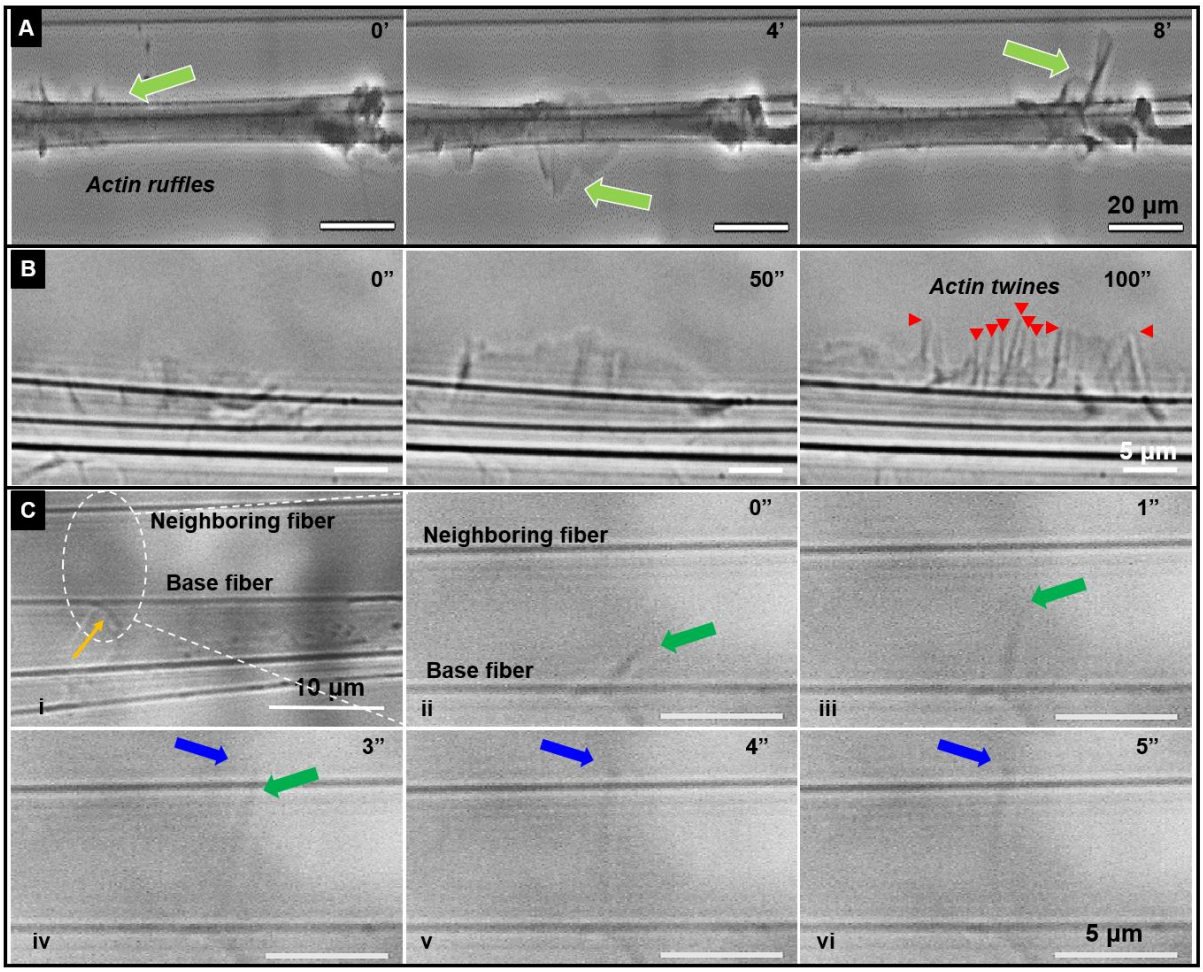

FIGURE 2. Anisotropic substrates enable twines to emerge from actin ruffles and engage neighboring fibers in seconds. Time-lapse images showing (A) Actin wave (green arrow) travelling along the length of cell body (Movie M2). (B) Actin wave ruffles develop into striated structures leading to formation of nano-filamentous '*twine*s' shown by red arrowheads (Movie M3). (C) i. Image of a cell with *twine* shown by yellow arrow. (ii-vi) Time-lapse images of area indicated by dashed oval demonstrating that *twine* engagement with neighboring fiber takes place in ~seconds (Movie M4). Green arrow shows growth of *twine* from cell body and blue arrow shows *twine* growth after engagement with neighboring fiber i.e. overhanging part of *twine*.

Discreet steps in the formation of perpendicular lateral protrusions (PLPs)

We inquired how *twine* structures matured (became thicker). Usage of 63X magnification and 1 s imaging allowed us to identify and quantitate formation of secondary *twines* and *twine-bridges* (**Movie M4**). We observed formation of force exerting PLP to occur in seven (7) characteristic steps (**Figure 3A(a,b)**). Step (i) Cells stretch on anisotropic fibers ('base fibers') in elongated morphologies. Step (ii) The base fibers serve as anchors enabling the cell to probe for neighboring fibers by extending rigid "probing twines," lateral protrusions that lunge outwards, and sway from their base to encounter a neighboring fiber. Twines engage with a neighboring fiber (**Figure 2c**). Step (iii) Cell extends a triangular lamellum anchored between twine and the base fiber. Step (iv) From the lamellum, one or more 'secondary twines' are formed similar to folding and buckling driven stratification of membrane ruffle described before. Step (v) Secondary twines then lunge and reach towards the neighboring fiber. When at least one makes contact and adheres to the neighboring fiber, which has primary twine attached to it, the two twines act as anchors, and the cell begins to fills in space between itself and the neighboring fiber with actin, thus forming a suspended 'twine-bridge,' which can be of different shapes (**Figure 3B**). Step (vi) After the twine bridge completely fills the space

between the cell and neighboring fiber (forming an 'interfiber lamellum'), the twine-bridge widens with a classic hour-glass shape (timepoint 6 minutes in **Figure 1**). Step (vii) As twine-bridge widens, they apply inward contractile forces thus deflecting the neighboring fiber. The original neighboring fiber can now serve as a new base fiber, thus perpetuating fibroblastic expansion and increased contraction.

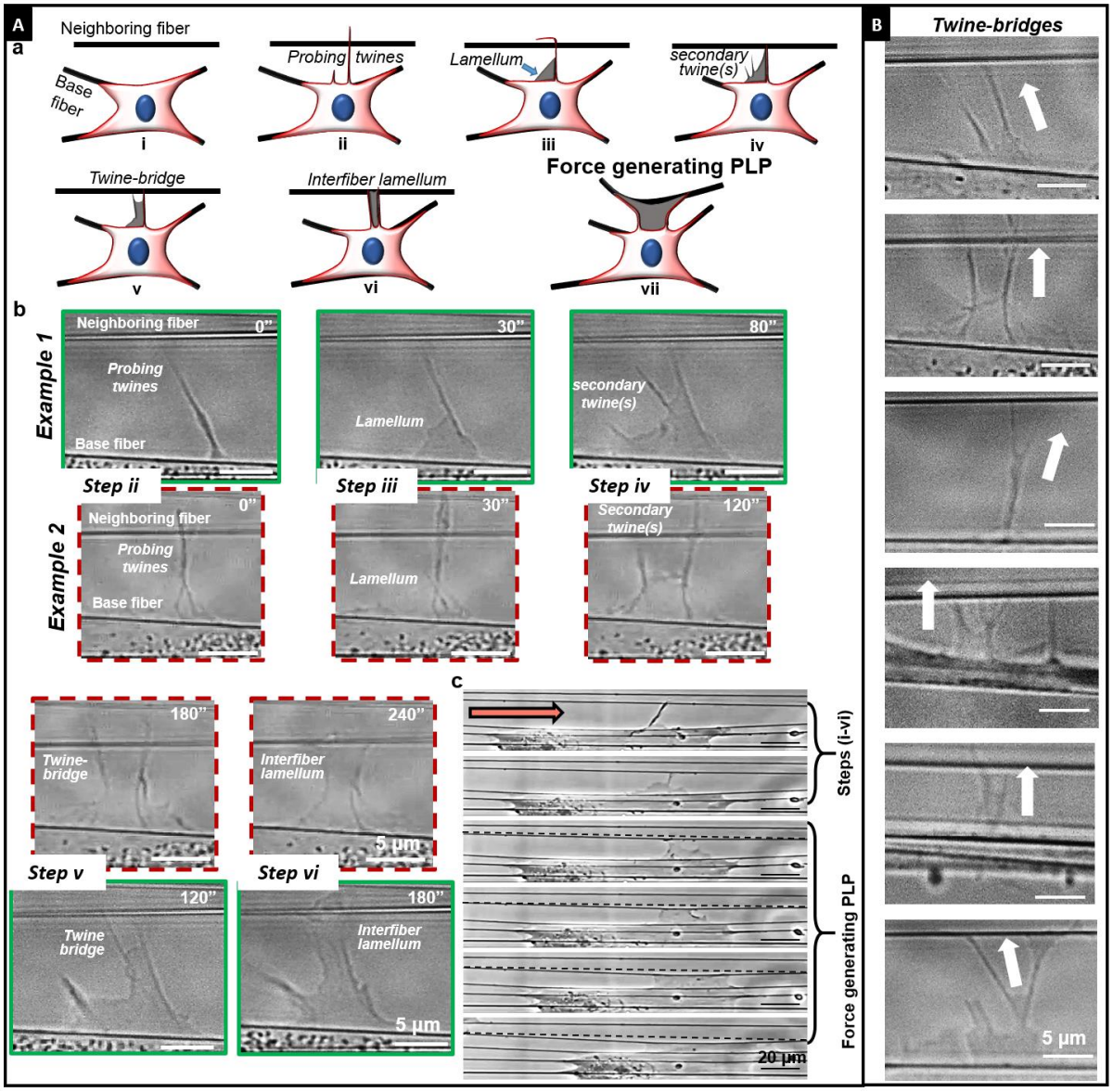

FIGURE 3. Discreet steps in formaiton of force exerting perpendicular lateral protrusions (PLPs). (A) a) Cartoons showing the process of forming force exerting perpendicular lateral protrusions (PLPs). Cells attached to fibers form filamentous *twines* that engage with with neighboring fiber (i). Subsequently, actin lamellum grows along the base of *twine* from cell body (ii) followed by formation of secondary *twines* (iii). Engagement of secondary *twine* with neighboring fiber leads to formation of a suspended *twine-bridge* (iv) that facilitates advancement of actin that generates a suspended *interfiber lamellum* (v). Over time (~minutes), the interfiber lamellum broadens and applies contractile forces causing neighboring fiber tocontract inwards, thus creating force exerting PLPs(vii). Phase images in green and red (dashed) boxes depict two sample cases of PLPs in steps (i-vi). (c) Phase images of whole cell forming PLP. Red dashed lines indicate undeflected position of neighboring fiber. Orange arrow indicates cell migration direction. (B) Sample images of *twine-bridges* of varying sizes and shapes and arrows point towards the neighboring fiber.

Actin based growth, location, and orientation of PLPs

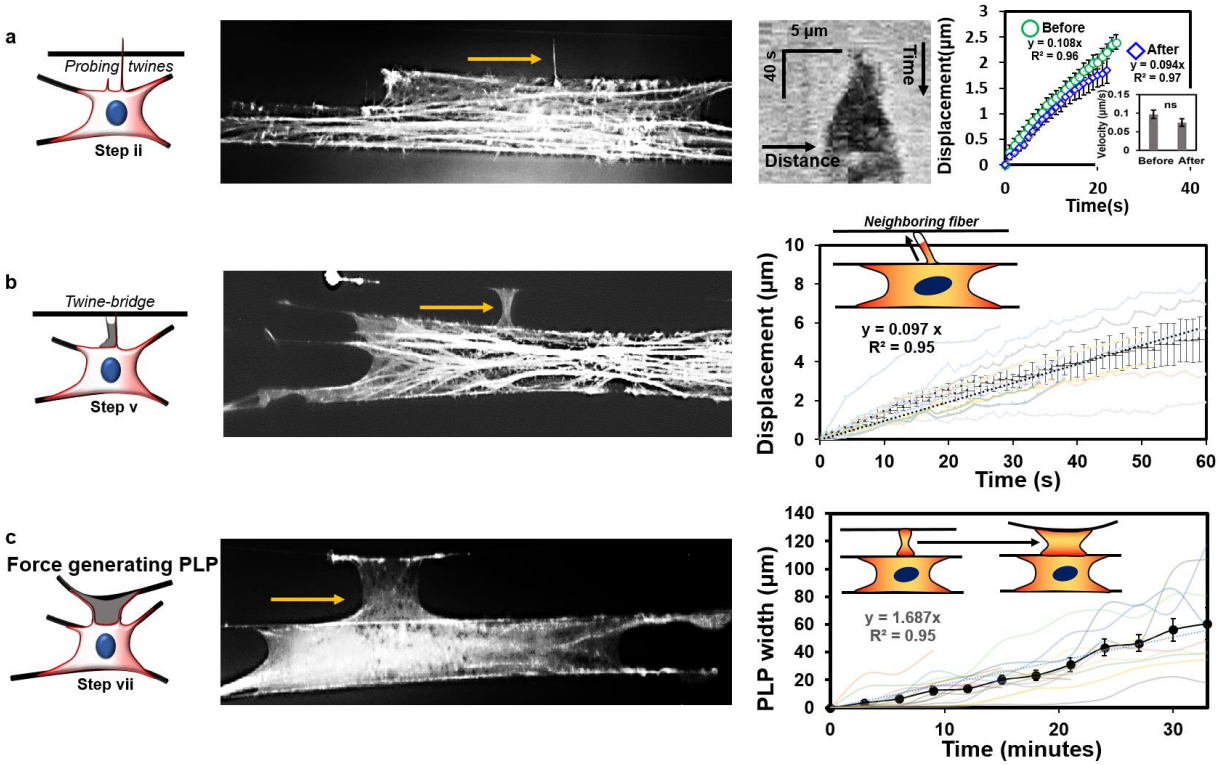

FIGURE 4. Actin kinetics in PLP formation. (a)Twines attached to neighboring fibers grow in width along the neighboring fiber axis as demonstrated by the kymograph obtained by performing line scan along the fiber axis. The average displacement vs. time profiles of advancement of *twine* before and after engagement with neighboring fiber (n=17 for both). Inset shows average velocity for the two categories. (b) Displacement vs. time profiles showing extension rates of actin lamellum between *twine-bridges* (n=13). Inset shows cartoon of actin lamellum advancement along the *twine-bridge*. (c) Broadening of twine-bridge into force exerting PLP (n=15). Data for linear fits to average of all profiles in included in each plot.

Filopodial extensions and their transition to lamellipodial structures are well-known to be driven by actin dynamics at the leading edge. We inquired if the twine-PLP transition was also actin-based (**Figure 4**). We recorded the growth rate of primary twines as they emerged from actin ruffles and found them to extend at ~0.1 µm/s, which matches the reported kinetics of filopodia extension rate (~0.12-0.2 µm/s[43]), and post engagement with neighboring fibers, the *twines* continued to grow at rates similar to pre-engagement (inset in **Figure 4a**). Next, we analyzed the growth of lamellum in the twine-bridges and found the lamellum to advance at the rate of ~0.1 µm/s (**Figure 4b**), similar to actin polymerization rates (~0.12-0.14 µm/s).[37] We saw that *twine-bridges* could mature into contractile force exerting structures (PLPs) as they broadened. We measured the width of twine-bridges halfway along their span length and found them to widen at ~0.028 µm/s (**Figure 2a(vii)**), which matched the actin retrograde flow rates (~0.008-0.025 µm/s in the lamellipodial tip) but much faster than the flowrate reported in lamella (~0.004-0.008 µm/s).[44] Overall, our measurements of twine, lamellum and twine-bridge widening match reported values of actin dynamics, thus suggesting twine-PLP transitions are similar to actin-based filopodial-lamellipodial transitions.

Next, we recorded that *twines* and PLPs of varying lengths (5-35 µm) formed along the entire length of the cell body (**Figure 5a**). Intriguingly, we found that while *twines* attached to neighboring fibers over a wide range of angles, the ensuing PLPs were recorded to be primarily oriented orthogonal to the parent cell body (**Figure 5b**). We also inquired if the spatial organization of *twines* and PLPs were exclusive to cells attached to anisotropic fiber networks. We constructed three more designs (hexagonal, angled, and crosshatches: **Movies M5-7**) and recorded the number of *twines* (length ≥ 3 µm) forming in cells in each fiber category. We found that the highest number of *twine* formation per cell over a two-hour period (imaged

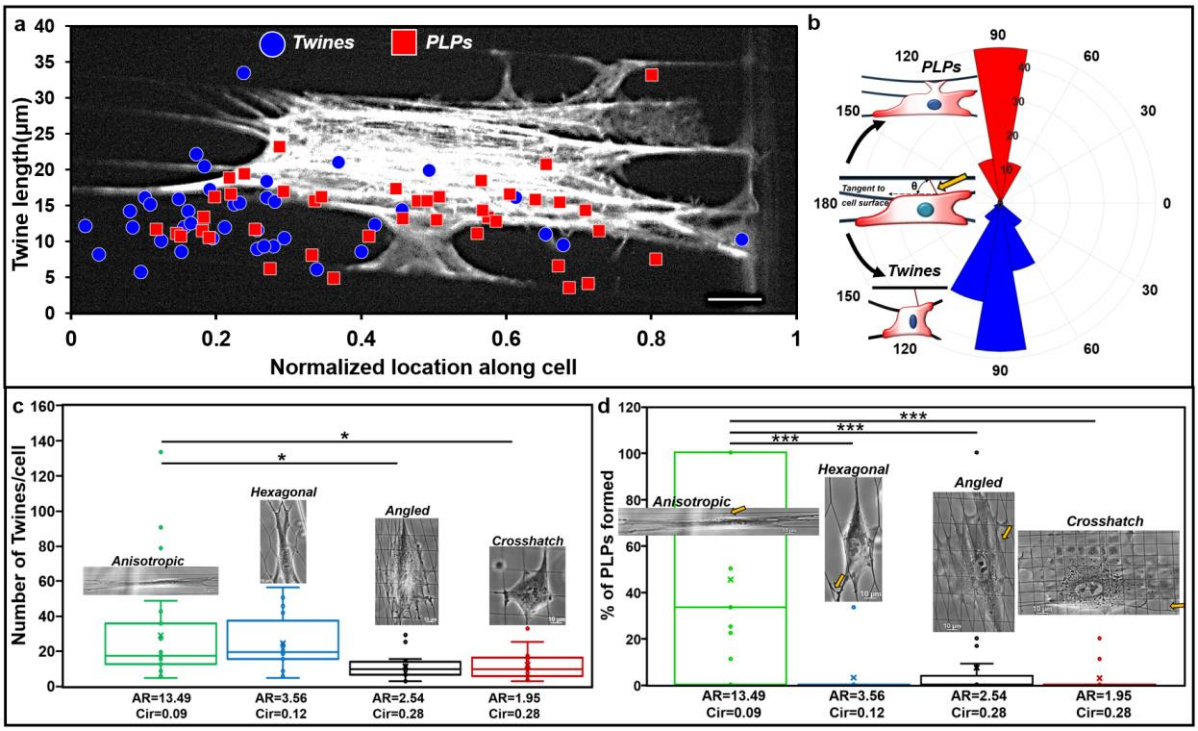

FIGURE 5. ***Twine and PLPs.*** (a) Plot showing the length of *twine*s observed with respect to corresponding location of emergence of *twines* and PLPs along the normalized cell length. Backdrop shows a cell forming multiple lateral protrusions. Scale bar 10 µm. (b) Polar histogram of angle formed by *twine or PLP* engagement axis and a tangent to cell body (n=84 for PLP and 123 for *twines*). PLPs are oriented perpendicularly to cell body. (c-d) Four fiber network designs were created to interrogate cell shape (AR: aspect ratio and Circ.: circularity) driven number density of (i) *twines,* and (ii) *PLP* formation ((number of PLPs/number of attached twines)*100). Elongated cells of high aspect ratios and small circularities form maximum number of twines/cell on anisotropic and hexagonal networks, while only anisotropic networks facilitate formation of PLPs. Data is analyzed from 23 randomly selected videos for each category.

every two minutes) occurred in elongated cells with high aspect ratios (observed on anisotropic and hexagonal structures, **Figure 5c**). Since *twines* were attaching to neighboring fibers in all categories, we calculated the number of PLPs formed from these attached *twines* (**Figure 5d**). Not surprisingly, we found that on average, nearly half of engaged *twines* transitioned to PLPs in cells attached to anisotropic parallel fibers, whereas for all other fiber networks, we rarely encountered formation of PLPs. Altogether, our data demonstrate that the maximum number of actin-based twines are formed in elongated cell shapes, but the transition of these twines to force exerting PLPs almost exclusively occurs in anisotropic arrangement of fibers.

Forces of *twine-bridges* and PLPs

It is now well-appreciated that cells *in vivo* and in 3D interstitial ECM exert contractile forces on the neighboring fibrous environments either by pushing or tugging at individual fibers.[18,45,46] In a similar manner, we also observed that *twines* that transitioned to broad lamellipodial resembling structures were able to pull neighboring fibers inwards towards the cell body, thus allowing the cells to spread on multiple fibers. Thus, we inquired the development of forces in PLPs and consequential migratory and force response of cells as they spread from three to four and five fibers using PLPs.

First, we quantitated the forces exerted by both *twines* and PLPs using Nanonet Force Microscopy (NFM[34,35], **Figure 6A**) through the establishment of *realistic* tension bearing force vectors directed towards the cell body. Specifically, the vectors originate at the paxillin attachments and point along the membrane

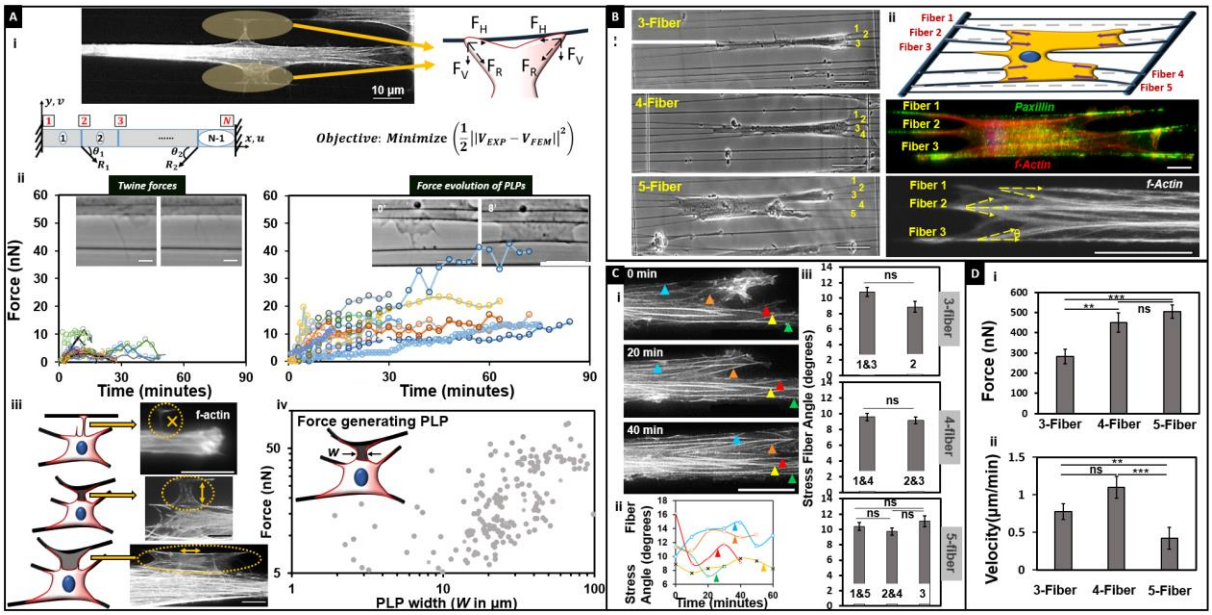

FIGURE 6. **Forces applied by *twine-bridges* facilitate cell spreading**. (A) i. Representative *twine-bridges* (scale bar 10 µm) along with representation of forces exerted by developing *twine-bridge*. Force vectors are assumed to act along the membrane curvature with origin at paxillin cluster lengths. To evaluate the forces, the deflected fiber is modelled as beam with fixed-fixed boundary condition. The force vectors R_1 and R_2 are calculated by minimizing the objective function, where V_{EXP} represents the displacement profile of the beam measured from image sequences and V_{FEM} is the prediction from finite element model. ii. Force response of *twine-bridges* over time for undeveloped and developed category with inset images showing both categories. Developing *twine-bridges* allow cells to spread across multiple fibers. (iii) f-actin stress fibers in twines, twine-bridges and PLPs shown in dashed yellow ovals. Arrows indicate direction of f-actin stress fibers, while cross indicates lack of or poorly developed stress fibers in twines. Scale bars 10 µm. (iv) Forces in developing twine-bridges show a sharp increase in force generation beyond 10 µm width of twine-bridge (W) shown in the cartoon. (B) i. Representative phase images of anisotropically stretched cells on 3, 4 and 5 fibers. ii. Schematic representation of NFM method to measure contractile forces of single cells attached to multiple fibers. The direction of force vectors are determined from paxillin focal adhesion clustering (FAC shown by green) acting along f-actin stress fibers (red and white). (C) i. Time-lapse images showing stress fibers tracked for angular measurements in a cell attached to five fibers. ii. Triangles of different colors in fluorescent image correspond to the transient plot. Measurements of all stress fibers could not be taken for the entire one-hour period as the respective cell front migrated out of the field of view. iii. The average f-actin stress fiber angle data: 3-fiber category: fiber 1&3 (n=53, n signifying number of stress fibers), fiber 2 (n=30). 4-fiber category: fiber 1&4 (n=80), fiber 2&3 (n=84). 5-fiber category: fiber 1&5 (n=72), fiber 2&4 (n=70), fiber 3 (n=35). (D) i. Average of total force calculated for 3 time points separated by 3 minutes each for spread cells selected randomly (n=13, 14 & 15 for 3, 4 & 5 fiber categories respectively). ii. Average migration rates for each fiber category (n=15 in each). Scale bar is (A) 20µm, (C)i. 50µm and ii. 20µm, (D)i. 20 µm.

curvature in twine-bridges and PLPs. For twine-bridges less than 6 µm in width, a single force vector pointing vertically towards the parent cell body was assigned, while two force vectors on either side of twine-bridges were assigned for sizes greater than six µm. We classified the ability of twines to exert force if they deflected the neighboring fibers ≥2 µm. Forces are estimated using a custom finite-element model that minimizes the difference between experimental data (measured fiber displacement profile) and model prediction (**Figure 6a(i)**). Our analysis revealed that *twines* angled from the parent cell body could apply forces for only a brief period, which prevented their maturation into broad lamellipodial PLP structures (**Figure 6a(ii)**). However, we found that angled twines could transition to force exerting PLPs when the angle transitioned close to 90 degrees due to the movement of the cell body (**Movie M8**). Immunostaining for f-actin stress fibers within the lateral protrusions showed that the stress fibers in twine-bridges were oriented along the length of the twine-bridge, and those in PLPs were oriented along the axis of parent cell body (yellow arrows in **Figure 6a(iii)**). We did not observe well defined f-actin stress fibers in twines. Force generation increased with twine-bridge width (W, measured at the middle of span length and shown in the

cartoon in **Figure 6a(iv)**), and for PLPs of widths greater than 10 µm, we observed a sharp increase in force generation presumably due to well-defined organization of stress fibers and their alignment with the parent cell body. Overall, our force analysis indicates that transition of f-actin stress fiber orientation from orthogonal (in twines and twine-bridges) to in line with cell elongation axis (in PLPs) suggests neighboring fiber to become a new base fiber for further cell spreading.

Next, since cells were using *PLPs* in anisotropic cell migration to spread onto neighboring fibers, we inquired how the *inside-out* contractile state of cells changed when they spread from 3 to 4 and 5 fibers (**Figure 6B(i)**). For the calculation of forces applied by cells, we approximated a strategy of using a single force vector that originated at the site of paxillin focal adhesion clustering (FAC) and pointed along the dominant f-actin stress fiber (**Figure 6B(ii)**). We chose this strategy based upon our previous finding that cells attached to ~250 nm diameter fibers formed focal adhesion clusters (FAC) at the poles.[34] We quantified the transient change in stress fiber angles as cells migrated and observed the stress fibers to maintain their relative positions (**Figure 6C(i,ii)**, **Supplementary figure S2** and **Movie M9**). Overall, the stress fibers were found on average to be angled between 8-11 degrees (**Figure 6C(iii)**). The overall contractile force was computed by summation of the individual forces acting at the adhesion clusters ($F_{Cell} = \sum F_{FAC}$). Cells spread on 5 fibers exerted higher forces (~505 nN), and as a consequence had statistically lower migration rates compared to those on 3 (~282 nN) or 4 fibers (~451 nN) (**Figure 6D**). We found that cells attached to fibers had a symmetric distribution of forces with the highest contractility driven by fibers at the outermost boundaries of cells (**Supplementary figure S3**).

DISCUSSIONS and CONCLUSIONS

It is long thought that scarring in wound healing and desmoplastic fibrotic ECM in cancer share similarities in causative origins, and newer findings point to fibroblasts as key culprits. Aligned extracellular fibers in these environments allow metastatic invasion and persistent cell migration. In contrast, the physiologically normal stroma is naturally randomly oriented and tumor suppressive[47–49]. Strategies to ablate the culprit cancer associated fibroblasts (CAF) have indeed reduced stroma but offered no benefit to pancreatic ductal adenocarcinoma (PDAC) patients[50], or in some cases even dangerously promoted cancer progression[51,52]. Thus, there is growing appreciation for “stroma normalization,” i.e. reinstitution of physiological ECM, and not its elimination that is expected to impart clinical benefit[48,53–57]. A direct route to achieve stroma normalization is first understanding the biophysical links that perpetuate desmoplastic expansion, and second develop informed intervention strategies that dissuade this expansion. In this study, we describe a new functional role of anisotropic environments, which enables elongated fibroblasts to spread and continually fuel desmoplastic expansion. We show for the first time that fibroblastic cells can form contractile force generating perpendicular lateral protrusions (PLPs) anywhere along the length of the body that contract neighboring fibers.

PLPs are formed in an orchestrated chain of events starting from actin ruffles that give rise to microspikes and filopodia resembling primary *twines*. Twines lunge and attach to neighboring fibers in a matter of seconds, which is in agreement with a recent study showing fibroblasts adhering to fibronectin in ≤ 5s in an α5β1-integrin-dependent manner.[58] While microspikes and filopodia rarely exceed lengths of ~10 µm,[59] the lengths of *twine*s observed by us had wide distribution (short ~ 5 µm to extremely long ~ 35 µm). To the best of our knowledge, filopodia of similar or longer lengths have been reported only in the case of sea urchin embryos.[60] Filopodia in cells cultured on 2D substrates localize at the leading edge, and can transition to broad lamellipodial structures. Filopodia-lamellipodial transitions that occur at sides of cells on 2D are usually associated with cell turning. In contrast, we discover that in anisotropic fibers, filopodial twines are oriented orthogonal to parent cell, and their transition to lamellipodial PLP never change cell migration direction. Instead, PLPs apply inward contractile forces that enable the cell to stretch in lateral direction resulting in an overall elongated cell shape over increased number of fibers.

The parallel fibers used in our method mimic the aligned ECMs produced by cancer associated fibroblasts (CAFs) *in vitro* and *in vivo* $TACs_{2/3}$ fiber configurations known to enable CAF activation[11,61]. The

inter-fiber spacing (~10 µm) used in our study mimics those measured by the fibroblastic cell-derived ECMs model and single harmonic generation (SHG) imaging of the patient samples[7,9,11,61–63]. At higher inter-fiber spacing[64,65], cells attach to single fibers in spindle morphologies with limited instances of twine formation, akin to the behavior reported in elongated spindles in 3D gels[15]. We also used three different fiber architectures: hexagonal, angled and crosshatch, to determine the efficacy of network designs in the formation of PLPs. Parallel and hexagonal networks support persistent cell migration in elongated shapes, while angled and crosshatch networks induce spread shapes and random migration. Elongated cell shapes on hexagonal and parallel networks form the maximum number of twines that can engage with neighboring fibers. However, only parallel fibers have the highest propensity to support formation of force generating PLPs. Thus, we emphasize that ECM architecture and elongated cell shape are key physical determinants of desmoplastic expansion.

Using parallel fibers also allows us to use them as force sensors. While individual filopodia have been shown in the past to exert forces (~2nN)[66], here using NFM we quantitate the transient force response of *twines* from thin to thick lamellipodial resembling structures capable of exerting higher forces (tens of nanonewton), thus providing the necessary support for cells to spread onto neighboring fibers. The increase in force generation in PLPs coincides with their increase in width (**Figure 6a(iv)**), which is correlated with the presence and spatial organization of f-actin stress fibers. Correlating the alignment of f-actin stress fibers with activation of phosphorylated focal adhesion kinase (pFAK) at adhesion sites on neighboring fibers will provide further evidence on formation of 3D adhesions and cells activating to force generating myofibroblasts.[61] We emphasize that our method of force measurement establishes force vectors originating from adhesion sites and directed along f-actin stress fibers contrasts other methods where the force vectors are determined independently of stress fiber orientation[67–69].

In conclusion, using NFM, we show in a reproducible and replicable manner that elongated cells on anisotropic fiber networks spread in the lateral direction through the formation of force generating lateral protrusions. Our findings identify a new cell behavior that describes the missing biophysical link in desmoplastic expansion of ECM. Further improvements in density, organization, and size of fibers coupled with RhoGTPase signaling in PLPs from any site on the cell body may provide intervention strategies to deter matrix-driven fibrous spread in cancers and chronic wounding diseases.

METHODS

Nanonet Manufacturing and Cell Culture:

The suspended polystyrene fibers were manufactured by the previously reported non-electrospinning STEP technique.[32,70] A network of small diameter parallel fibers (~250 nm) was deposited 5-7 µm apart upon a layer of base fibers (~ 1 µm) spaced 350 µm apart and fused at the interjections. The scaffolds were placed in glass bottom 6-well plates (MatTek, Ashland, MA) and sterilized in 70% ethanol for 10 min. After two rounds of PBS (1x) wash, 50 µl of 4µg/ml of Fibronectin (Invitrogen, Carlsbad, CA) was put on the scaffolds and incubated at 37°C for 30 min to facilitate cell adhesion. Bone Marrow-derived human Mesenchymal Stem Cells, hMSCs (Lonza Inc, Basel, Switzerland) were cultured in supplemented growth medium (Lonza Inc) at 37°C and 5% CO2. Cells were seeded on the scaffolds by placing 50 µl droplets of 100,000 cells/mL on the suspended part, and 300 µl of media was placed around the well to prevent evaporation. After incubation for 2hr to facilitate attachment, two mL of supplemented growth medium was added to each well.

Time Lapse Microscopy and Cell Force Calculations

Nanonets in 6 well plate were placed in an incubating microscope (AxioObserver Z1, Carl Zeiss, Jena, Germany). Time Lapse movies were created by taking images at 20x at 3min or 40/63X at the 1-second interval with an AxioCam MRm camera (Carl Zeiss). All measurements were performed using

AxioVision (Carl Zeiss) and ImageJ (National Institute of Health, Bethesda, MD). Using beam mechanics, cell forces were estimated from experimentally obtained deflection of fibers. Briefly, an optimization algorithm written in MATLAB (MathWorks, Natick, MA) matched the experimental and computational finite-element fiber deflections to calculate forces at each time point (for details on model development, optimization algorithm and validation tests see supplementary information).

Immunohistochemistry and Immunofluorescence Imaging

Cells on fibers were fixed in 4% paraformaldehyde, permeabilized in 0.1% Triton X100 solution and blocked in 5% goat serum. Paxillin staining was done using primary rabbit anti-paxillin antibodies (Invitrogen) at a dilution of 1:250 and incubated at 4°C for 1h. Secondary goat anti-rabbit Alex Fluor 488 (Invitrogen) antibodies were incubated for 45 min at room temperature in the dark. F-Actin stress fibers were stained using Rhodamine Phalloidin. Cell nuclei were stained with 300 nM of DAPI (Invitrogen) for 5 min. The scaffolds were kept hydrated in 2ml PBS (phosphate-buffered saline) during imaging. Fluorescent images were taken using an Axio Observer Z1 microscope (Carl Zeiss). Actin live cell imaging was performed as per manufacturer's instructions on using the reagent CellLight Actin-RFP, Bacman 2.0 (Invitrogen).

Statistical Analysis

Sample populations were tested for statistical significance using the Student's t-test and analysis of variance (ANOVA) for multiple group comparisons in GraphPad software (GraphPad Prism, California). Error bars represent standard errors. Values are reported as an average ± 1 SE. * denotes p-value ≤ 0.05, ** p-value ≤ 0.01, and *** denotes p-value ≤ 0.001.

ACKNOWLEDGMENTS

ASN, EC and KMH are thankful to late Professor Keely (University of Wisconsin) for discussions and guidance on cell biology and dedicate this manuscript in her remembrance. ASN would like to acknowledge the Institute of Critical Technologies and Sciences (ICTAS) at Virginia Tech for the support to conduct this study. AP and ASN would like to thank members of the STEP Lab for their helpful suggestions and discussions.

Declaration

The authors declare no competing interests.

Author Contributions

ASN, EC, and KMH designed research and intellectual conceptualization. ASN supervised the research. AP performed the experiments and conducted the analysis. AP, DM and JF analyzed the IF images. KS and RKK developed the analytical and finite element model. AP, EC, KMH and ASN wrote the manuscript.

Funding Sources

This work is supported by National Science Foundation (NSF 1437101 and 1462916) awarded to ASN.

REFERENCES

(1) Hinz, B.; Gabbiani, G. Mechanisms of Force Generation and Transmission by Myofibroblasts. *Curr. Opin. Biotechnol.* **2003**, *14*, 538–546.

(2) Hinz, B.; Mastrangelo, D.; Iselin, C. E.; Chaponnier, C.; Gabbiani, G. Mechanical Tension Controls Granulation Tissue Contractile Activity and Myofibroblast Differentiation. *Am. J. Pathol.* **2001**, *159*, 1009–1020.

(3) Dvorak, H. F. Tumors: Wounds That Do Not Heal. Similarities between Tumor Stroma Generation and Wound Healing. *N. Engl. J. Med.* **1986**, *315*, 1650–1659.

(4) Rybinski, B.; Franco-Barraza, J.; Cukierman, E. The Wound Healing, Chronic Fibrosis, and Cancer Progression Triad. *Physiol. Genomics* **2014**, *46*, 223–244.

(5) Alexander, J.; Cukierman, E. Stromal Dynamic Reciprocity in Cancer: Intricacies of Fibroblastic-ECM Interactions. *Curr. Opin. Cell Biol.* **2016**, *42*, 80–93.

(6) Erkan, M.; Michalski, C. W.; Rieder, S.; Reiser-Erkan, C.; Abiatari, I.; Kolb, A.; Giese, N. A.; Esposito, I.; Friess, H.; Kleeff, J. The Activated Stroma Index Is a Novel and Independent Prognostic Marker in Pancreatic Ductal Adenocarcinoma. *Clin. Gastroenterol. Hepatol.* **2008**, *6*, 1155–1161.

(7) Conklin, M. W.; Eickhoff, J. C.; Riching, K. M.; Pehlke, C. A.; Eliceiri, K. W.; Provenzano, P. P.; Friedl, A.; Keely, P. J. Aligned Collagen Is a Prognostic Signature for Survival in Human Breast Carcinoma. *Am. J. Pathol.* **2011**, *178*, 1221–1232.

(8) Goetz, J. G.; Minguet, S.; Navarro-Lérida, I.; Lazcano, J. J.; Samaniego, R.; Calvo, E.; Tello, M.; Osteso-Ibáñez, T.; Pellinen, T.; Echarri, A.; *et al.* Biomechanical Remodeling of the Microenvironment by Stromal Caveolin-1 Favors Tumor Invasion and Metastasis. *Cell* **2011**, *146*, 148–163.

(9) Bredfeldt, J. S.; Liu, Y.; Conklin, M. W.; Keely, P. J.; Mackie, T. R.; Eliceiri, K. W. Automated Quantification of Aligned Collagen for Human Breast Carcinoma Prognosis. *J. Pathol. Inform.* **2014**, *5*, 28.

(10) Conklin, M. W.; Gangnon, R. E.; Sprague, B. L.; Van Gemert, L.; Hampton, J. M.; Eliceiri, K. W.; Bredfeldt, J. S.; Liu, Y.; Surachaicharn, N.; Newcomb, P. A.; *et al.* Collagen Alignment as a Predictor of Recurrence after Ductal Carcinoma In Situ. *Cancer Epidemiol. Biomarkers Prev.* **2018**, *27*, 138–145.

(11) Amatangelo, M. D.; Bassi, D. E.; Klein-Szanto, A. J. P.; Cukierman, E. Stroma-Derived Three-Dimensional Matrices Are Necessary and Sufficient to Promote Desmoplastic Differentiation of Normal Fibroblasts. *Am. J. Pathol.* **2005**, *167*, 475–488.

(12) Provenzano, P. P.; Eliceiri, K. W.; Campbell, J. M.; Inman, D. R.; White, J. G.; Keely, P. J. Collagen Reorganization at the Tumor-Stromal Interface Facilitates Local Invasion. *BMC Med.* **2006**, *4*, 38.

(13) Provenzano, P. P.; Inman, D. R.; Eliceiri, K. W.; Trier, S. M.; Keely, P. J. Contact Guidance Mediated Three-Dimensional Cell Migration Is Regulated by Rho/ROCK-Dependent Matrix Reorganization. *Biophys. J.* **2008**, *95*, 5374–5384.

(14) Heck, J. N.; Ponik, S. M.; Garcia-Mendoza, M. G.; Pehlke, C. A.; Inman, D. R.; Eliceiri, K. W.; Keely, P. J. Microtubules Regulate GEF-H1 in Response to Extracellular Matrix Stiffness. *Mol. Biol. Cell* **2012**, *23*, 2583–2592.

(15) Riching, K. M.; Cox, B. L.; Salick, M. R.; Pehlke, C.; Riching, A. S.; Ponik, S. M.; Bass, B. R.; Crone, W. C.; Jiang, Y.; Weaver, A. M.; *et al.* 3D Collagen Alignment Limits Protrusions to Enhance Breast Cancer Cell Persistence. *Biophys. J.* **2014**, *107*, 2546–2558.

(16) Oudin, M. J.; Jonas, O.; Kosciuk, T.; Broye, L. C.; Guido, B. C.; Wyckoff, J.; Riquelme, D.; Lamar, J. M.; Asokan, S. B.; Whittaker, C.; *et al.* Tumor Cell-Driven Extracellular Matrix Remodeling Drives Haptotaxis during Metastatic Progression. *Cancer Discov.* **2016**, *6*, 516–531.

(17) Adams, J. C. Cell-Matrix Contact Structures. *Cell. Mol. Life Sci.* **2001**, *58*, 371–392.

(18) Wolf, K.; Friedl, P. Mapping Proteolytic Cancer Cell-Extracellular Matrix Interfaces. *Clin. Exp. Metastasis* **2009**, *26*, 289–298.

(19) Taylor, A. C.; Robbins, E. Observations on Microextensions from the Surface of Isolated Vertebrate Cells. *Dev. Biol.* **1963**, *7*, 660–673.

(20) Nourshargh, S.; Hordijk, P. L.; Sixt, M. Breaching Multiple Barriers: Leukocyte Motility through Venular Walls and the Interstitium. *Nat. Rev. Mol. Cell Biol.* **2010**, *11*, 366–378.

(21) McEver, R. P.; Zhu, C. Rolling Cell Adhesion. *Annu. Rev. Cell Dev. Biol.* **2010**, *26*, 363–396.

(22) Ramachandran, V.; Yago, T.; Epperson, T. K.; Kobzdej, M. M.; Nollert, M. U.; Cummings, R. D.; Zhu, C.; McEver, R. P. Dimerization of a Selectin and Its Ligand Stabilizes Cell Rolling and

Enhances Tether Strength in Shear Flow. *Proc. Natl. Acad. Sci. U. S. A.* **2001**, *98*, 10166–10171.
(23) Bruehl, R. E.; Springer, T. A.; Bainton, D. F. Quantitation of L-Selectin Distribution on Human Leukocyte Microvilli by Immunogold Labeling and Electron Microscopy. *J. Histochem. Cytochem.* **1996**, *44*, 835–844.
(24) Karnik, R.; Hong, S.; Zhang, H.; Mei, Y.; Anderson, D. G.; Karp, J. M.; Langer, R. Nanomechanical Control of Cell Rolling in Two Dimensions through Surface Patterning of Receptors. *Nano Lett.* **2008**, *8*, 1153–1158.
(25) Tozluoğlu, M.; Tournier, A. L.; Jenkins, R. P.; Hooper, S.; Bates, P. A.; Sahai, E. Matrix Geometry Determines Optimal Cancer Cell Migration Strategy and Modulates Response to Interventions. *Nat. Cell Biol.* **2013**, *15*, 751–762.
(26) Nelson, C. M.; Bissell, M. J. Of Extracellular Matrix, Scaffolds, and Signaling: Tissue Architecture Regulates Development, Homeostasis, and Cancer. *Annu. Rev. Cell Dev. Biol.* **2006**, *22*, 287–309.
(27) Petrie, R. J.; Doyle, A. D.; Yamada, K. M. Random versus Directionally Persistent Cell Migration. *Nat. Rev. Mol. Cell Biol.* **2009**, *10*, 538–549.
(28) Worthylake, R. a; Burridge, K. RhoA and ROCK Promote Migration by Limiting Membrane Protrusions. *J. Biol. Chem.* **2003**, *278*, 13578–13584.
(29) Pankov, R.; Endo, Y.; Even-Ram, S.; Araki, M.; Clark, K.; Cukierman, E.; Matsumoto, K.; Yamada, K. M. A Rac Switch Regulates Random versus Directionally Persistent Cell Migration. *J. Cell Biol.* **2005**, *170*, 793–802.
(30) Koons, B.; Sharma, P.; Ye, Z.; Mukherjee, A.; Lee, M. H.; Wirtz, D.; Behkam, B.; Nain, A. S. Cancer Protrusions on a Tightrope: Nanofiber Curvature Contrast Quantitates Single Protrusion Dynamics. *ACS Nano* **2017**, *11*.
(31) Nain, A. S.; Sitti, M.; Jacobson, A.; Kowalewski, T.; Amon, C. Dry Spinning Based Spinneret Based Tunable Engineered Parameters (STEP) Technique for Controlled and Aligned Deposition of Polymeric Nanofibers. *Macromol. Rapid Commun.* **2009**, *30*.
(32) Wang, J.; Nain, A. S. Suspended Micro/Nanofiber Hierarchical Biological Scaffolds Fabricated Using Non-Electrospinning STEP Technique. *Langmuir* **2014**, *30*, 13641–13649.
(33) Nain, A. S.; Phillippi, J. a; Sitti, M.; Mackrell, J.; Campbell, P. G.; Amon, C. Control of Cell Behavior by Aligned Micro/Nanofibrous Biomaterial Scaffolds Fabricated by Spinneret-Based Tunable Engineered Parameters (STEP) Technique. *Small* **2008**, *4*, 1153–1159.
(34) Sheets, K.; Wang, J.; Zhao, W.; Kapania, R.; Nain, A. S. Nanonet Force Microscopy for Measuring Cell Forces. *Biophys. J.* **2016**, *111*, 197–207.
(35) Hall, A.; Chan, P.; Sheets, K.; Apperson, M.; Delaughter, C.; Gleason, T. G.; Phillippi, J. A.; Nain, A. Nanonet Force Microscopy for Measuring Forces in Single Smooth Muscle Cells of the Human Aorta. *Mol. Biol. Cell* **2017**, *28*, 1894–1900.
(36) Terrier, C. G.; Monzo, P.; Zhu, J.; Long, H.; Venkatraman, L.; Zhou, Y.; Wang, P.; Chew, S. Y.; Mogilner, A.; Ladoux, B.; *et al.* Protrusive Waves Guide 3D Cell Migration along Nanofibers. **2015**, *211*.
(37) Giannone, G.; Dubin-Thaler, B. J.; Rossier, O.; Cai, Y.; Chaga, O.; Jiang, G.; Beaver, W.; D??bereiner, H. G.; Freund, Y.; Borisy, G.; *et al.* Lamellipodial Actin Mechanically Links Myosin Activity with Adhesion-Site Formation. *Cell* **2007**, *128*, 561–575.
(38) Pontes, B.; Monzo, P.; Gole, L.; Le Roux, A.-L.; Kosmalska, A. J.; Tam, Z. Y.; Luo, W.; Kan, S.; Viasnoff, V.; Roca-Cusachs, P.; *et al.* Membrane Tension Controls Adhesion Positioning at the Leading Edge of Cells. *J. Cell Biol.* **2017**, *216*, 2959–2977.
(39) Zidovska, A.; Sackmann, E. On the Mechanical Stabilization of Filopodia. *Biophys. J.* **2011**, *100*, 1428–1437.
(40) Tamada, A.; Kawase, S.; Murakami, F.; Kamiguchi, H. Autonomous Right-Screw Rotation of Growth Cone Filopodia Drives Neurite Turning. *J. Cell Biol.* **2010**, *188*, 429–441.
(41) Albrecht-Buehler, G. Filopodia of Spreading 3T3 Cells: Do They Have a Substrate-Exploring Function? *J. Cell Biol.* **1976**, *69*, 275–286.
(42) Bornschlögl, T. How Filopodia Pull: What We Know about the Mechanics and Dynamics of Filopodia. *Cytoskeleton* **2013**, *70*, 590–603.
(43) Mogilner, A.; Rubinstein, B. The Physics of Filopodial Protrusion. *Biophys. J.* **2005**, *89*, 782–795.
(44) Tomasello, M.; Kirby, S.; Polich, L.; Senghas, R. J.; Wanner, E.; Gleitman, L. R.; Morford, J. P.; Coppola, M.; Kegl, J.; Senghas, A.; *et al.* Two Distinct Actin Networks Drive the Protrusion Of. *Science (80-.).* **2004**, *305*, 1782–1787.

(45) Hodor, P. G.; Illies, M. R.; Broadley, S.; Ettensohn, C. A. Cell-Substrate Interactions during Sea Urchin Gastrulation: Migrating Primary Mesenchyme Cells Interact with and Align Extracellular Matrix Fibers That Contain ECM3, a Molecule with NG2-like and Multiple Calcium-Binding Domains. *Dev. Biol.* **2000**, *222*, 181–194.
(46) Wyckoff, J. B.; Pinner, S. E.; Gschmeissner, S.; Condeelis, J. S.; Sahai, E. ROCK- and Myosin-Dependent Matrix Deformation Enables Protease-Independent Tumor-Cell Invasion In Vivo. *Curr. Biol.* **2006**, *16*, 1515–1523.
(47) Rybinski, B.; Franco-Barraza, J.; Cukierman, E. The Wound Healing, Chronic Fibrosis, and Cancer Progression Triad. *Physiological Genomics*, 2014, *46*, 223–244.
(48) Schnittert, J.; Bansal, R.; Prakash, J. Targeting Pancreatic Stellate Cells in Cancer. *Trends in cancer* **2019**, *5*, 128–142.
(49) Park, C. C.; Bissell, M. J.; Barcellos-Hoff, M. H. The Influence of the Microenvironment on the Malignant Phenotype. *Molecular Medicine Today*, 2000, *6*, 324–329.
(50) Kim, E. J.; Sahai, V.; Abel, E. V; Griffith, K. A.; Greenson, J. K.; Takebe, N.; Khan, G. N.; Blau, J. L.; Craig, R.; Balis, U. G.; *et al.* Pilot Clinical Trial of Hedgehog Pathway Inhibitor GDC-0449 (Vismodegib) in Combination with Gemcitabine in Patients with Metastatic Pancreatic Adenocarcinoma. *Clin. Cancer Res.* **2014**, *20*, 5937–5945.
(51) Cannon, A.; Thompson, C.; Hall, B. R.; Jain, M.; Kumar, S.; Batra, S. K. Desmoplasia in Pancreatic Ductal Adenocarcinoma: Insight into Pathological Function and Therapeutic Potential. *Genes Cancer* **2018**, *9*, 78–86.
(52) Hirata, E.; Sahai, E. Tumor Microenvironment and Differential Responses to Therapy. *Cold Spring Harb. Perspect. Med.* **2017**, *7*, 1–14.
(53) Whittle, M. C.; Hingorani, S. R. Fibroblasts in Pancreatic Ductal Adenocarcinoma: Biological Mechanisms and Therapeutic Targets. *Gastroenterology* **2019**, *156*, 2085–2096.
(54) Sherman, M. H.; Yu, R. T.; Engle, D. D.; Ding, N.; Atkins, A. R.; Tiriac, H.; Collisson, E. A.; Connor, F.; Van Dyke, T.; Kozlov, S.; *et al.* Vitamin D Receptor-Mediated Stromal Reprogramming Suppresses Pancreatitis and Enhances Pancreatic Cancer Therapy. *Cell* **2014**, *159*, 80–93.
(55) Neesse, A.; Krug, S.; Gress, T. M.; Tuveson, D. A.; Michl, P. Emerging Concepts in Pancreatic Cancer Medicine: Targeting the Tumor Stroma. *Onco. Targets. Ther.* **2013**, *7*, 33–43.
(56) Neesse, A.; Bauer, C. A.; Öhlund, D.; Lauth, M.; Buchholz, M.; Michl, P.; Tuveson, D. A.; Gress, T. M. Stromal Biology and Therapy in Pancreatic Cancer: Ready for Clinical Translation? *Gut* **2019**, *68*, 159–171.
(57) Bigelsen, S. Evidence-Based Complementary Treatment of Pancreatic Cancer: A Review of Adjunct Therapies Including Paricalcitol, Hydroxychloroquine, Intravenous Vitamin C, Statins, Metformin, Curcumin, and Aspirin. *Cancer Manag. Res.* **2018**, *10*, 2003–2018.
(58) Strohmeyer, N.; Bharadwaj, M.; Costell, M.; Fässler, R.; Müller, D. J. Fibronectin-Bound A5β1 Integrins Sense Load and Signal to Reinforce Adhesion in Less than a Second. *Nat. Mater.* **2017**, *16*, 1262–1270.
(59) Saarikangas, J.; Zhao, H.; Pykäläinen, A.; Laurinmäki, P.; Mattila, P. K.; Kinnunen, P. K. J.; Butcher, S. J.; Lappalainen, P. Molecular Mechanisms of Membrane Deformation by I-BAR Domain Proteins. *Curr. Biol.* **2009**, *19*, 95–107.
(60) Mattila, P. K.; Lappalainen, P. Filopodia: Molecular Architecture and Cellular Functions. *Nat. Rev. Mol. Cell Biol.* **2008**, *9*, 446–454.
(61) Franco-Barraza, J.; Francescone, R.; Luong, T.; Shah, N.; Madhani, R.; Cukierman, G.; Dulaimi, E.; Devarajan, K.; Egleston, B. L.; Nicolas, E.; *et al.* Matrix-Regulated Integrin Avβ5 Maintains A5β1-Dependent Desmoplastic Traits Prognostic of Neoplastic Recurrence. *Elife* **2017**, *6*.
(62) Malik, R.; Luong, T.; Cao, X.; Han, B.; Shah, N.; Franco-Barraza, J.; Han, L.; Shenoy, V. B.; Lelkes, P. I.; Cukierman, E. Rigidity Controls Human Desmoplastic Matrix Anisotropy to Enable Pancreatic Cancer Cell Spread via Extracellular Signal-Regulated Kinase 2. *Matrix Biol.* **2019**, *81*, 50–69.
(63) Robinson, B. K.; Cortes, E.; Rice, A. J.; Sarper, M.; Del Río Hernández, A. Quantitative Analysis of 3D Extracellular Matrix Remodelling by Pancreatic Stellate Cells. *Biol. Open* **2016**, *5*, 875–882.
(64) Sheets, K.; Wunsch, S.; Ng, C.; Nain, A. S. Shape-Dependent Cell Migration and Focal Adhesion Organization on Suspended and Aligned Nanofiber Scaffolds. *Acta Biomater.* **2013**, *9*, 7169–7177.
(65) Sharma, P.; Ng, C.; Jana, A.; Padhi, A.; Szymanski, P.; Lee, J. S. H.; Behkam, B.; Nain, A. S. Aligned Fibers Direct Collective Cell Migration to Engineer Closing and Nonclosing Wound Gaps. *Mol. Biol. Cell* **2017**, *28*, 2579–2588.

(66) Bridgman, P. C.; Dailey, M. E. The Organization of Myosin and Actin in Rapid Frozen Nerve Growth Cones. *J. Cell Biol.* **1989**, *108*, 95–109.
(67) Beningo, K. A.; Wang, Y. L. Flexible Substrata for the Detection of Cellular Traction Forces. *Trends Cell Biol.* **2002**, *12*, 79–84.
(68) Steinwachs, J.; Metzner, C.; Skodzek, K.; Lang, N.; Thievessen, I.; Mark, C.; Münster, S.; Aifantis, K. E.; Fabry, B. Three-Dimensional Force Microscopy of Cells in Biopolymer Networks. *Nat. Methods* **2016**, *13*, 171–176.
(69) Cesa, C. M.; Kirchgessner, N.; Mayer, D.; Schwarz, U. S.; Hoffmann, B.; Merkel, R. Micropatterned Silicone Elastomer Substrates for High Resolution Analysis of Cellular Force Patterns. *Rev. Sci. Instrum.* **2007**, *78*, 034301.
(70) Jana, A.; Nookaew, I.; Singh, J.; Behkam, B.; Franco, A. T.; Nain, A. S. Crosshatch Nanofiber Networks of Tunable Interfiber Spacing Induce Plasticity in Cell Migration and Cytoskeletal Response. *FASEB J.* **2019**, fj.201900131R.